Synthesis and characterization of a family of Fe(II) tetrazole complexes [Fe(C$_6$mtz)$_6$]X$_2$ (X = BF$_4^-$, ClO$_4^-$, PF$_6^-$)

Myrvete Tafili-Kryeziu, Andrea Caneschi, Maria Fittipaldi, Gabriele Spina, Marco Lantieri, Matthias Weil, Miki Hasegawa & Wolfgang Linert

Taylor & Francis
Taylor & Francis Group

Synthesis and characterization of a family of Fe(II) tetrazole complexes [Fe(C$_6$mtz)$_6$]X$_2$ (X = BF$_4^-$, ClO$_4^-$, PF$_6^-$)

MYRVETE TAFILI-KRYEZIU†, ANDREA CANESCHI‡, MARIA FITTIPALDI§,
GABRIELE SPINA§, MARCO LANTIERI¶, MATTHIAS WEIL‖, MIKI HASEGAWA††
and WOLFGANG LINERT*†

†Institute of Applied Synthetic Chemistry, Vienna University of Technology, Vienna, Austria
‡LAMM, Dipartimento di Chimica & UdR INSTM, Università di Firenze, Sesto Fiorentino (Fi), Italy
§LAMM, Dipartimento di Fisica ed Astronomia & UdR INSTM, Università di Firenze, Sesto Fiorentino (Fi), Italy
¶Istituto dei Sistemi Complessi, CNR, Sesto Fiorentino (Fi), Italy
‖Institute of Chemical Technologies and Analytics, Vienna University of Technology, Vienna, Austria
††College of Science and Engineering, Aoyama Gakuin University, Sagamihara, Japan
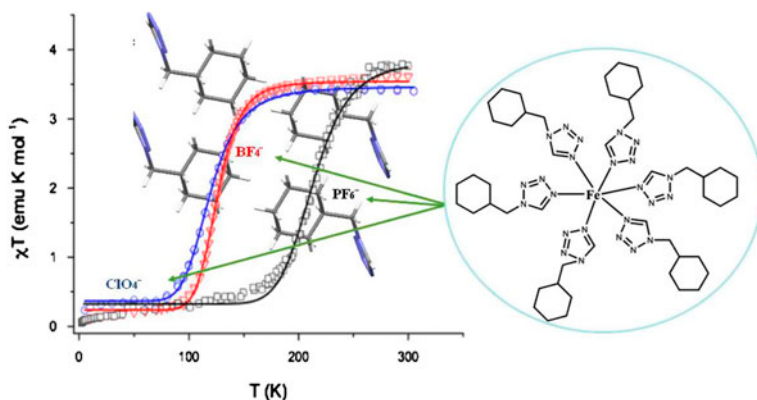
Based on 1-(cyclohexylmethyl)-1H-tetrazole (C$_6$mtz), a series of mononuclear iron(II) spin-cross-over complexes with the general formula [Fe(C$_6$mtz)$_6$]X$_2$, where X is the non-coordinating anion BF$_4^-$ (**1**), ClO$_4^-$ (**2**), or PF$_6^-$ (**3**), have been synthesized and characterized. Temperature-dependent magnetic susceptibility measurements for **1**, **2**, and **3** show reversible one-step spin crossover (SCO) behavior between high-spin (HS, $S = 2$) and low-spin (LS, $S = 0$) states without hysteresis. The PF$_6^-$ compound shows spin transition at $T_{1/2} = 213$ K at a considerably higher temperature than the other compounds, BF$_4^-$ ($T_{1/2} = 126$ K) and ClO$_4^-$ ($T_{1/2} = 119$ K). Temperature-dependent Far-IR and Mössbauer spectra of **2** and **3** were compared with the measured magnetic susceptibility and confirm the one-step SCO behavior of the compounds.

Keywords: Fe(II) complexes; Tetrazole; Magnetic properties; Temperature-dependent Far-IR spectroscopy; Mössbauer spectroscopy

*Corresponding author. Email: wolfgang.linert@tuwien.ac.at

1. Introduction

New magnetic materials have earned growing interest due to their potential technological importance, such as applications as memory devices, molecular sensors, or optical switches [1–3]. Metal ions with electron configuration d^4–d^7 in octahedral coordination geometry exhibit attractive properties such as spin transitions between the high-spin (HS) and low-spin (LS) states, depending on the distribution of the valence d electrons over the t_{2g} and e_g orbitals. One of these states is the ground state, and the other is a metastable state. This change of the spin state can be initiated by different external perturbations such as changes in temperature [4–6] or pressure [7–11], irradiation with light [12–14], or application of a magnetic field [15]. Since the first spin-crossover systems, Fe(III) dithiocarbamates, were reported by Cambi *et al.* in 1931 [16] a large number of new spin-crossover (SCO) compounds containing transition metal ions, mostly Fe(II) [17] and Fe(III) [18] and in a few cases Co(II), Cr(II), Mn(II), Mn(III) and Co(III) [19, 20], have been synthesized and investigated. In particular, Fe(II) complexes showing SCO behavior are of interest. The nature of the spin transition behavior between the HS and LS states of the compounds is influenced by type of ligand, the presence of solvent molecules in the crystal structure, or the nature of the counter-anion [21]. Interesting SCO properties with one or two-steps and wide hysteresis loops have been found using a limited number of the ligands such as imidazole, pyridine, pyrazole, triazole, and tetrazole derivatives.

In recent years, iron(II) SCO compounds using 1-substituted cycloalkyl tetrazoles have been published [22, 23]. $[Fe(C_3tz)_6](BF_4)_2$, with the rigid cyclopropyl substituent on the tetrazole, shows an abrupt and complete spin transition at $T_{1/2} = 190$ K [22], followed by the cyclohexyl-substituted compound $[Fe(C_6tz)_6](BF_4)_2$ at $T_{1/2} = 210$ K, whereas with a cyclopentyl-substituent, $[Fe(C_5tz)_6](BF_4)_2$ shows only an incomplete and gradual spin transition behavior [23].

For deeper insight into the factors which influence the spin transition behavior, we synthesized and investigated the more flexible 1-cyclohexylmethyl-1H-tetrazole (C_6mtz) and a series of Fe(II) complexes with general formula $[Fe(C_6mtz)_6]X_2$, where X is the non-coordinating anion BF_4^- (**1**), ClO_4^- (**2**), or PF_6^- (**3**). Accordingly, temperature-dependent magnetic data of the mentioned iron(II) complexes, accompanied by Mid-IR, and temperature-dependent Far-IR spectra of **3** and Mossbauer spectra of **2**, are reported.

2. Experimental

2.1. *Chemicals and physical characterization*

Sodium azide (99%), triethylorthoformate (99%), glacial acetic acid (99%), and cyclohexyl-methylamine (98%) were obtained from Alfa Aesar. Iron(II) tetrafluoroborate-hexahydrate (97%), iron(II) perchlorate-hydrate (98%), iron(II) chloride-tetrahydrate (99%), and silver hexafluorophosphate (98%) were obtained from Aldrich. All other chemicals were standard reagent grade and used as supplied.

2.2. *Physical measurements*

Elemental analyses (C, H, and N) were performed on a Perkin Elmer 2400 CHN Elemental Analyzer. The characterization of the ligand was accomplished by NMR spectroscopy: ^{1}H

spectra in $CDCl_3$ measured with a Bruker DPX-200 MHz and ^{13}C spectra at 50 MHz. The chemical shifts are reported in ppm calibrated to the respective solvent. Mid-range IR spectra of the compounds were recorded with the attenuated total reflectance (ATR) technique from 4000 to 450 cm^{-1} using a Perkin–Elmer Spectrum Two FTIR spectrometer with a UATR accessory attached. Variable temperature far-IR spectra have been measured from 700 to 100 cm^{-1} with a Perkin Elmer Spectrum 400 FIR/MIR FTIR spectrometer using polyethylene pellets. The polyethylene pellets of the sample holder with silicon windows were recorded between 100 and 300 K. Pellets were obtained by pressing the powdered mixture of the samples in polyethylene in vacuo using a Carver 4350.L hydraulic press and by applying a pressure of approx. 10.000 kg cm^{-2} for 5 min. To obtain a reasonable signal to noise ratio, 600 scans were totaled for each spectrum. The sample temperature was allowed to equilibrate for 10 min before each measurement. Temperature-dependent magnetic susceptibility measurements were performed from 2 to 300 K with an applied field of 1 T using a Cryogenic S600 SQUID magnetometer. Raw data were corrected for the contribution of the sample holder, measured in the same field and temperature range, and the intrinsic diamagnetism of the sample, estimated by Pascal's constants. The magnetic susceptibility has been evaluated as $\chi = M/H$ and corrected for temperature-independent paramagnetic contributions (TIP).

Mössbauer measurements were performed using a Wissel™ spectrometer, calibrated by a standard metal iron foil, and a nitrogen-based Oxford™ flux cryogenic system with a base temperature of 67 K at 232 mbar. The Mössbauer source was a 25 mCi $^{57}Co/Rh$ sample with a Lamb–Mössbauer factor $f_s = 0.63$, which was evaluated by applying the method described [24]. The prepared sample contained 193 mg cm^{-2} of active material, corresponding roughly to the ideal quantity for a single-line absorber, as calculated following the procedure detailed [25]. The absorber thickness $t_a = n_a\sigma_0\beta f_a(T)$ [26], where n_a is the number of iron ions per cm^2, β is the ^{57}Fe isotopic abundance, σ_0 is the maximum resonant cross section and f_a is the absorber Lamb–Mössbauer factor, was expected to be $\approx 5.1 f_a(T) \approx 3$ at low temperatures, by assuming $f_a = f_s$, which represents the Lamb–Mössbauer factor of the source. Therefore, spectra are expected to be affected by saturation effects. It is not convenient to reduce the amount of active material in the absorber, since strong decreases of f_a occur in organic molecular compounds by increasing T. However, spectra with $t_a \approx 3$ should be correctly handled by means of the integral transmission method [27]. The fitting procedure requires evaluation of the reduced Mössbauer source factor $f_s^{(r)}$ that multiplies the convolution integral. This parameter is derived, for each Mössbauer spectrum, from the source recoilless fraction f_s throughout the collection of additional pulse height analysis spectra [24]. The accuracy of the fitting procedure was tested by comparing $n_a\sigma_0\beta f_a(T)$, which was evaluated by fitting the Mössbauer spectra, with the value expected on the basis of the quantity of compound in the target.

Single crystal structure determination of 1-(cyclohexylmethyl)-1H-tetrazole has been performed. A preselected single crystal of $C_8H_{14}N_4$ was mounted with a high-viscosity perfluorinated polyether on a thin silica glass fiber and cooled on a Bruker AXS APEXII CCD four-circle diffractometer (Mo Kα radiation with graphite monochromator) in a dry stream of nitrogen to 100 K. The data collection strategy was optimized with the APEX2 [28] software using the complete reciprocal sphere up to 29°/2θ, leading to a highly redundant dataset. Correction of absorption effects after integration of the data with SAINT [28] was performed with the semi-empirical "multi-scan" approach using SADABS [28]. The crystal structure of $C_8H_{14}N_4$ was solved by direct methods and refined by full covariance matrix least-squares methods on F^2 using the SHELXTL package [29]. The cyclohexylmethyl moi-

Table 1. Details for the crystal structure determination of $C_8H_{14}N_4$.

Temperature (K)	100
λ (Å)	0.71073
Formula	$C_8H_{14}N_4$
Formula weight	166.23
Crystal description	light-yellow plate
Crystal dimensions	$0.50 \times 0.25 \times 0.02$
Crystal system	triclinic
Space group	P$\bar{1}$
a (Å)	5.5439(3)
b (Å)	5.5779(3)
c (Å)	15.6277(11)
α (°)	93.220(5)
β (°)	97.731(5)
γ (°)	110.646(4)
V (Å^3)	445.31(5)
Z	2
$F(0\,0\,0)$	180
ρ_{calc} (g cm^{-3})	1.240
μ (mm^{-1}) (Mo Kα)	0.080
Coefficients of transmission T_{min}; T_{max}	0.9609; 0.9984
Number of reflections measured	6607
Number of independent reflections	2275
Number of reflections with $I > 2\sigma(I)$	174
R_{int}	0.0273
θ_{min}, θ_{max}	2.65; 29.00
H	$-7 \rightarrow 7$
K	$-7 \rightarrow 7$
L	$-21 \rightarrow 21$
$\Delta\rho_{max}$ (e Å^{-3})	0.34
$\Delta\rho_{min}$ (e Å^{-3})	-0.25
$R[I > 2\sigma(I)]$, all	0.0393, 0.0595
$wR2[I > 2\sigma(I)]$, all	0.0938, 0.1048
Goof	1.028

ety is disordered over two sites with an occupancy ratio of 0.725(3) : 0.275(3). The disordered groups were refined with similarity restraints (DELU and SIMU) [29] to achieve sensible bond lengths and displacement parameters for the minor component. All non-H atoms were refined with anisotropic displacement parameters. The aromatic hydrogen of the tetrazole group was clearly discernible from a difference Fourier map, but was finally positioned geometrically and refined in the riding model approximation with a C–H distance restraint of 0.95 Å and $U_{iso}(H) = 1.2\ U_{eq}(C)$ of the parent. Methylene and methine hydrogens of the cyclohexylmethyl moiety were also positioned geometrically, with C–H distances of 0.99 and 1.0 Å, respectively, and with $U_{iso}(H) = 1.2\ U_{eq}(C)$. Crystallographic data and details of the X-ray data collection and structure refinement are listed in table 1.

2.3. *Synthesis of the ligand*

Warning: Tetrazoles and their derivatives are potentially shock-sensitive or explosive compounds and must be handled with care (scheme 1).

Synthesis of the ligand was carried out according to the literature method [30] with some modifications. Cyclohexylmethylamine (5 g, 44.16 mmol),) triethyl orthoformate (9.81 g, 66.24 mmol and sodium azide (4.3 g, 66.24 mmol) were dissolved in 40 mL of acetic acid
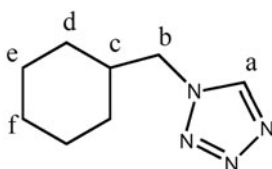
Scheme 1.   Assignments of ^{13}C NMR data of 1-(cyclohexylmethyl)-1H-tetrazole.

and heated at 75 °C for 45 h. After evaporation of acetic acid and excess orthoformate under reduced pressure, the residue was dissolved in water and extracted with chloroform. The combined organic layers were washed with water and saturated aqueous solutions of $NaHCO_3$ and NaCl. After drying the organic phase over Na_2SO_4 and evaporation of the solvent under reduced pressure, the crude product, a semi-solid, was formed. The crude product was recrystallized in acetone and after storing in the freezer at low temperature (−24 °C), white crystals precipitated. The product was recovered by filtration and washed with cold ethanol. Yield 4.06 g (55.3%). Anal. Calcd for $C_8H_{14}N_4$ (%): C 57.81; H 8.49; N 33.71. Found: C 58.76; H 8.56; N 32.91. ^{1}H NMR (200 MHz, $d_1 − CDCl_3$, 25 °C): δ: 8.54 (s, 1H), 4.25 (d, $J = 7.06$ Hz, 2H), 1.97 (m, $J = 3.67$ Hz, 3H), 1.68 (m, $J = 7.61$, 4H), 1.19 (m, $J = 7.46$, 4H) ppm. ^{13}C NMR (50 MHz, $d_1 − CDCl3$, 25 °C): δ: 142.94 (CaH-tz), 54.42 (Cb), 38.38 (Cc), 30.37 (2Cd), 25.95 (Cf), 25.43 (2Ce) ppm. IR (ATR): $v_{C–H\ (tz)} = 3115$ cm^{-1}.

Single crystals of 1-(cyclohexylmethyl)-1H-tetrazole (C_6mtz) were grown by re-crystallization of the product from n-hexane and subsequent slow evaporation of the solvent at room temperature.

2.4. *Synthesis of the complexes*

All iron(II) compounds were synthesized under nitrogen and using standard Schlenk techniques.

2.4.1. Synthesis of [Fe(C$_6$mtz)$_6$](X)$_2$, where X = BF$_4^-$, ClO$_4^-$. 1-(Cyclohexylmethyl)-1H-tetrazole (0.498 g, 3 mmol) was dissolved in 5 mL of ethanol, and Fe(BF$_4$)$_2$·6H$_2$O (0.169 g, 0.5 mmol) or Fe(ClO$_4$)$_2$·H$_2$O (0.127 g, 0.5 mmol) (respectively) was dissolved in 10 mL ethanol and a small amount of ascorbic acid [to avoid oxidation of iron(II)]. The iron solution was dropwise added to the ligand solution at room temperature and stirred for a few hours. The solvent was reduced under a stream of argon at room temperature. After keeping the solution one day at −24 °C, a white precipitate was formed. The product was recovered by filtration, washed with cold ethanol and dried. **[Fe(C$_6$mtz)$_6$](BF$_4$)$_2$** Yield: 0.187 g (30%). Anal. Calcd for $C_{48}H_{84}B_2F_8FeN_{24}$ (%): C 46.99; H 6.90; N 27.40. Found: C 46.58; H 6.65; N 26.72. IR (ATR): $v_{C–H\ (tz)} = 3136$ cm^{-1}. **[Fe(C$_6$mtz)$_6$](ClO$_4$)$_2$** Yield: 0.217 g (35%). Anal. Calcd for $C_{48}H_{84}Cl_2O_8FeN_{24}$ (%): C 46.04; H 6.76; N 26.85. Found: C 46.32; H 6.66; N 26.31. IR (ATR): $v_{C–H\ (tz)} = 3129$ cm^{-1}.

2.4.2. Syntheses of [Fe(C$_6$mtz)$_6$](PF$_6$)$_2$ complex. 1-(Cyclohexylmethyl)-1H-tetrazole (0.498 g, 3 mmol) was dissolved in 5 mL ethanol and FeCl$_2$·4H$_2$O (0.099 g, 0.5 mmol)

dissolved in 7 mL ethanol and a small amount of ascorbic acid (to avoid oxidation of iron (II)) was dropwise added to the solution of the ligand. After 10 min. stirring, ethanol solution of $AgPF_6$ (0.25 g, 1 mmol) was dropwise added, whereupon AgCl immediately precipitated. After 1 h of stirring at 40 °C, the AgCl was removed by filtration and washed with ethanol. The filtrate was reduced under a stream of argon at room temperature. After keeping the solution one day at low temperature (−24 °C), a white precipitate was formed. The precipitate was recovered by filtration, washed with cold ethanol and dried. Yield: 0.3552 g (53%). Anal. Calcd. for $[Fe(C_6mtz)_6](PF_6)_2$ $C_{48}H_{84}P_2F_{12}FeN_{24}$ (%): C 42.92; H 6.30; N 25.03. Found: C 42.55; H 6.07; N 24.74. IR (ATR): $\nu_{C-H\ (tz)} = 3159$ cm^{-1}.

3. Results and discussion

3.1. *Synthesis and crystal structures*

1-(Cyclohexylmethyl)-1H tetrazole − $C_8H_{14}N_4$ − crystallizes with two formula units in the triclinic system in space group P$\bar{1}$. The cyclohexyl ring of the cyclohexylmethyl moiety has a chair conformation; bond length and angles in the cyclohexylmethyl and tetrazole moieties are in the normal ranges (figure 1). The crystal packing (figure 2) is supported by π…π stacking interactions between parallel tetrazole rings of two adjacent molecules with a centroid…centroid distance of 3.342 Å (plane-to-plane distance 3.249 Å). Weak C–H…N hydrogen bonding interactions between two adjacent tetrazole rings (C1…N4 3.236(2) Å) and between the methyl of the cyclomethyl moiety and a neighboring tetrazole group (C2 … N2 3.517 Å) may also lead to a stabilization of the crystal structure.

Various attempts with different solvents to grow single crystals suitable for X-ray structure determination of the iron(II) compounds, failed. X-ray powder diffraction measurements of microcrystalline materials of **1** (BF_4^-), **2** (ClO_4^-) and **3** (PF_6^-) prepared
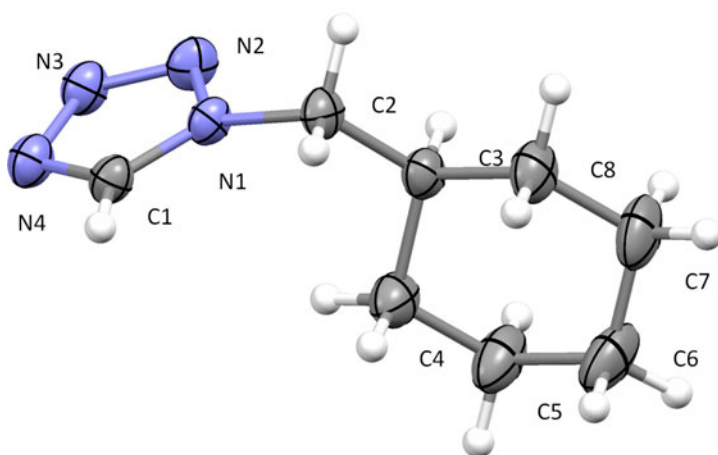

Figure 1. The molecular structure and atom labeling of $C_8H_{14}N_4$. Only the major part of the disordered cyclohexylmethyl moiety is shown. Displacement ellipsoids are drawn at the 70% probability level; hydrogens are displayed as spheres of arbitrary radius.
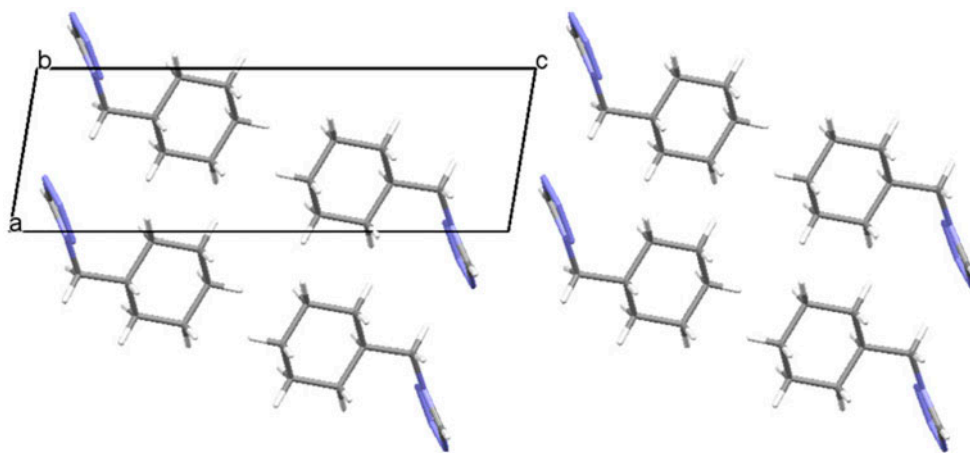
Figure 2.   The crystal packing of C8H14N4 viewed along the *b*-axis.

from ethanol were measured on a Panalytical X'Pert diffractometer in the Bragg–Brentano geometry using Cu K$\alpha_{1,2}$ radiation, a X'Celerator linear detector with a Ni-filter, sample spinning with backloading sample holders and $2\theta = 5$–$70°$ at room temperature. Unfortunately, only preliminary data of **3** (PF$_6^-$) could be refined. The diffractogram is presented in supplementary material figure S1. [Fe(C$_6$mtz)$_6$](PF$_6$)$_2$ crystallizes in the rhombohedral R-3 space group and provided preliminary unit cell parameters $a = 11.0964$, $c = 50.1105$, $V = 5343, 5083$ Å^3.

3.2. *Spectroscopic characterization of the ligand and the series of complexes*

Mid-IR spectra for the free ligand and the series of complexes were performed between 4000 and 450 cm^{-1}. Successful complexation is shown by significant differences of vibrational modes of the free ligand and bonded ligand in the complexes (figure 3). The stretching vibration ($\nu_{C-H\ (tz)}$) of the tetrazole is shifted to higher wavenumbers in the complex by about 21 cm^{-1} for the BF$_4^-$ compound to 14 cm^{-1} for the ClO$_4^-$ and 44 cm^{-1} for the PF$_6^-$ (see table 2). For more details of the mid – IR spectra, see the supplementary material figure S2–S5.

3.3. *Magnetic susceptibility measurements*

Temperature-dependent magnetic susceptibility for **1**, **2,** and **3** are shown in figure 4. The compounds show thermochromism; in the high-spin state, they are colorless and in the low-spin state, they are violet. The observed room temperature χT values are 3.17, 3.21, 3.23 emu K mol^{-1} for ClO$_4^-$, BF$_4^-$, PF$_6^-$ derivatives, respectively, which indicate an essentially full population of the $^5T_{2g}$ state for all three samples. On lowering temperature, clear evidence of spin state transition is observed for the three derivatives, leading to a low temperature χT value of 0.29, 0.10, 0.08 emu K mol^{-1}, suggesting either an incomplete transition to low-spin state, or traces of iron(III). Both of these situations often occur in SCO systems. However, Mossbauer spectroscopy (see below) tends to favor the former
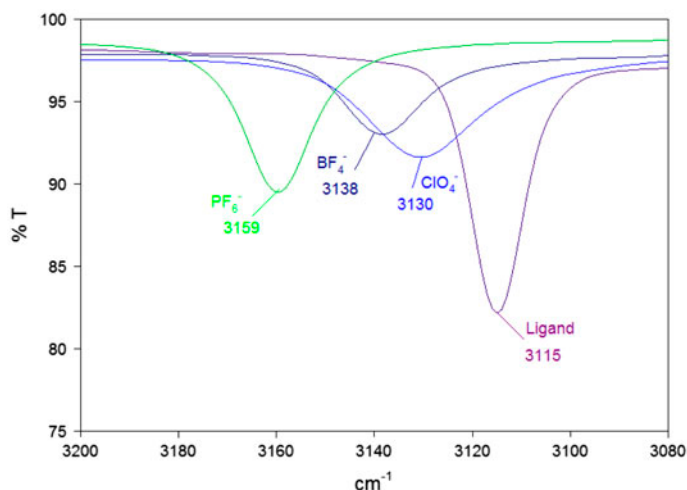
Figure 3.   Mid-IR spectra for free ligand and the series of complexes: violet for ligand (—), dark blue (—) for BF_4^- complex, blue (—) for ClO_4^- x and green (—) for PF_6^- complex (see http://dx.doi.org/10.1080/00958972.2015. 1077951 for color version).

Table 2.   Comparison of mid – IR spectra of C–H tz (tetrazol) bands between free ligand and the series of complexes.

	Complexes $\nu_{C-H\ (tz)}$ (cm^{-1})	Free ligand $\nu_{C-H\ (tz)}$ (cm^{-1})	Δ (cm^{-1})
[Fe(C$_6$mtz)$_6$](BF$_4$)$_2$	3136	3115	21
[Fe(C$_6$mtz)$_6$](ClO$_4$)$_2$	3129	3115	14
[Fe(C$_6$mtz)$_6$](PF$_6$)$_2$	3159	3115	44

hypothesis. Repeated cycles of heating/cooling did not evidence any hysteresis, ruling out appreciable cooperativity among neighboring molecules. Following these considerations, transition temperatures could be estimated by fitting the χT *versus* T curves assuming Boltzmann distribution among the two states, and the presence of a temperature-independent fraction of HS-Fe(II):

$$\chi T = \chi T_{HS-Fe^{II}} \left[\rho + \left(1 + \exp\left(\frac{\Delta H - T\Delta S}{RT} \right) \right)^{-1} (1 - \rho) \right] \tag{1}$$

where ΔH and ΔS are the enthalpic and entropic contributions to the crossover transition, and ρ is the percentage of paramagnetic impurity remaining at low temperature. The transition temperatures were estimated as $T_{1/2} = \Delta H/\Delta S$, which provided the values of 119 ± 1, 126 ± 1, 215 ± 2 K for the three complexes (with $\rho = 0.09$, 0.04, 0.04, respectively). The corresponding thermodynamic quantities obtained by best fit of the curves for the three derivatives were as follows: $\Delta H = 9.1 \pm 0.1$, 13.9 ± 0.2, 24.8 ± 0.9 kJ mol^{-1}; $\Delta S = 76 \pm 1$, 110 ± 2, 115 ± 4 J K^{-1} mol^{-1} for **1, 2,** and **3,** respectively.
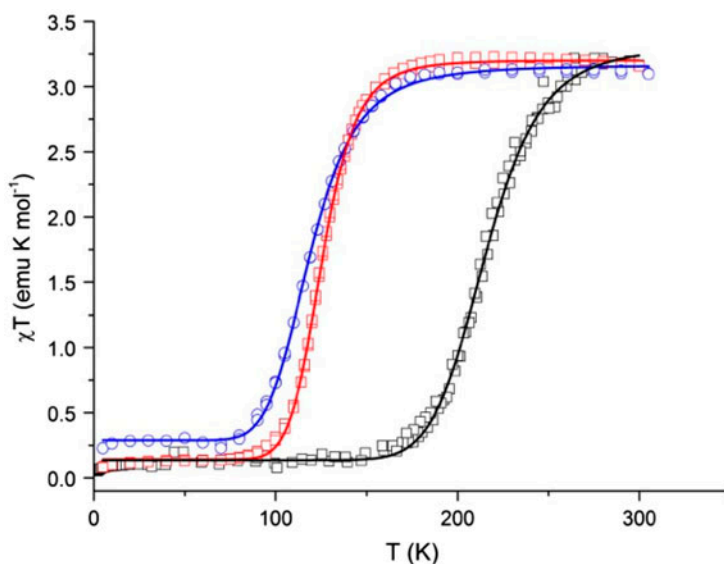
Figure 4. Temperature-dependent magnetic susceptibility of $[Fe(C_6mtz)_6](BF_4)_2$ (red squares $\triangle$), $[Fe(C_6mtz)_6]$ $(ClO_4)_2$ (blue circles $\circ$), $[Fe(C_6mtz)_6](PF_6)_2$ (black squares $\square$) in the form of χMT *vs. T* plots. Continuous line represents the best fit to equation (1) for the three derivatives using the parameters reported in the text (see http:// dx.doi.org/10.1080/00958972.2015.1077951 for color version).

3.4. *Temperature-dependent Far-IR spectroscopy of $[Fe(C_6mtz)_6](PF_6)_2$*

Variable temperature Far-IR spectroscopy is an ideal tool to observe the change of the N–Fe–N bond strength due to the spin transition and can be used to verify the SCO behavior obtained by magnetic measurements. The Far-IR spectra of **3** have been investigated as polyethylene pellets of the sample in the spectral range 700–100 cm^{-1} and the temperature range between 100 and 300 K at intervals of 10 K. At low temperature, the prominent vibration bands for the LS compound appear at 422, 384, and 360 cm^{-1} (see figure 5), while at room temperature, the vibration bands at 316 and 260 cm^{-1} correspond to bonding between the coordinating nitrogen of the tetrazole ligands and the iron(II) in the high-spin state. The band at 558 cm^{-1} corresponds to PF_6^- anion vibrations; the intensity increases with increasing temperature. The band at 220 cm^{-1} at room temperature shifts to 216 cm^{-1} at low temperature and does not disappear completely at 100 K [21a]. The high-spin molar fraction was calculated from the vibration bands at 220 and 260 cm^{-1} and found to be in agreement with the high-spin molar fraction obtained from magnetic measurements (see figure 6).

3.5. *^{57}Fe-Mössbauer spectroscopy of $[Fe(C_6mtz)_6](ClO_4)_2$*

Twelve standard transmission spectra (see figure 7) were collected on 1024 channels with $v_{max} = 3$ mm s^{-1} between 70 and 294 K, starting from a liquid nitrogen bath at 232 mbar. Since the experimental line shapes are clearly wider than the theoretical expected values and show a thermal evolution, inhomogeneous effects and/or small line shape distortions due to dynamical processes should be taken into account. Consequently, the Mössbauer
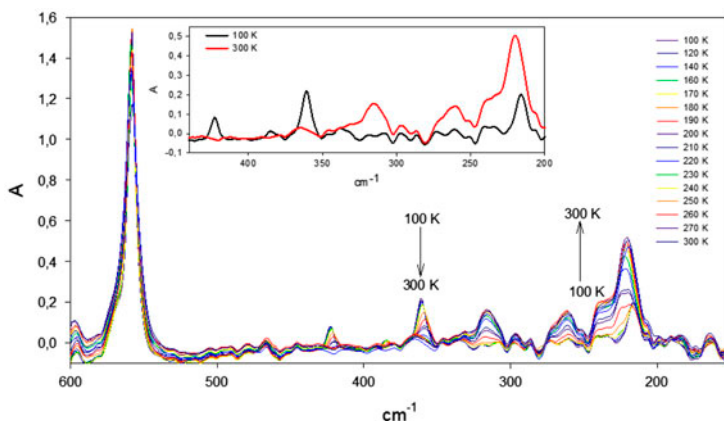
Figure 5. Variable temperature Far-IR spectra of $[Fe(C_6mtz)_6](PF_6)_2$ from 100 to 300 K. The insert shows the graph of Far-IR spectra of the LS state at 100 K and HS state at 300 K.
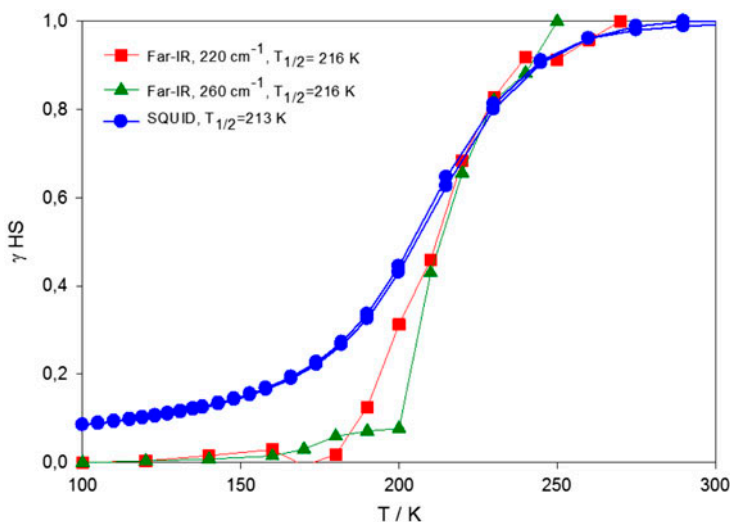

Figure 6. Comparison of the temperature-dependent high-spin molar fractions calculated from the magnetic measurements (●), variable temperature Far-IR (■, ▲) spectra of $[Fe(C_6mtz)_6](PF_6)_2$.

cross section, which is due to the HS and LS components and which appears in the transmission integral function, was expressed by a sum of Voigt doublets [33] and not by simple Lorentzian doublets. Each Voigt component was identified by four parameters: the contribution t_i to the absorber thickness number t_a, the center shift δ_i, the quadrupolar splitting Δ_i and, finally, the Gaussian component σ_i of the Voigt profile. In turn, the Lorentzian component of each doublet of the cross section was fixed at the natural value ≈ 0.1 mms^{-1}. Therefore, σ_i does not denote the FWHM of a single line, which is approximately given by $2\Gamma_n + 2\sigma_i\sqrt{2\ln 2} + 0.27\Gamma_n t_i$, where the last term is due to saturation [31]. Moreover, the
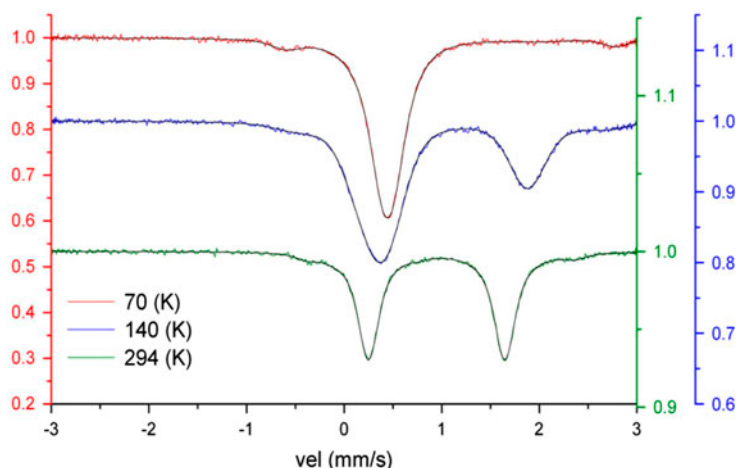
Figure 7. Experimental ^{57}Fe-Mössbauer spectra of $[Fe(C_6mtz)_6](ClO_4)_2$ collected at 70, 140, and 294 K plotted together with the corresponding curve fits. Due to the presence of not negligible saturation effects, Mossbauer spectra and cross section contributions are plotted separately in figure 8.

source line shape was described by a Voigt profile, the Gaussian component of which was determined by starting from the source FWHM indicated by the manufacturer.

The line shape of the spectra consists of a main component, which shows the typical SCO behavior from HS to LS states, and of a secondary HS-Fe(II) component ($\approx$5%), which is almost independent on *T*. Due to its spectral feature, we attribute the latter contribution to an impurity of a species with a different coordination environment, most probably due to an incomplete coordination of Fe(II) by C_6mtz.

We fitted the secondary component by means of a Voigt doublet and the SCO component by means of three Voigt doublets. Two of them are connected with the component of the main spin state (HS-Fe(II) over 120 K and LS-Fe(II) under 120 K), and the third one is related to the minor spin state (LS-Fe(II) over 120 K and HS-Fe(II) under 120 K).

The fit of the spectra reveals that the Gaussian broadenings of the Voigt doublets, belonging to the SCO component, depends on *T*. These broadenings do not practically contribute to the cross section line widths for those temperatures which lie at the extremes of the investigated range, and this result indicates that the saturation effects on the shape of the collected spectra have been accurately handled. At intermediate temperatures, we observe the FWHM of the Mossbauer cross section to increase to values on the order of $2\Gamma_n$ (see table 3 and cross sections reported in figure 8). Moreover, the HS contribution is reproduced by an asymmetrically broadened doublet. This feature suggests that the SCO-time window lies on the top of the Mössbauer time window (10^{-7} s) [32].

For *T* > 120 K an anomalous decrease of t_a is observed, also, although full analysis of this result goes far beyond the scope of the present article. By fitting the absorber thickness $t_a = \Sigma_i t_i$ by means of the Debye model (figure 9) for $T \leq 120$ K, we obtained $\theta_D = 168(8)$ K and $n_a\sigma_0\beta = 5.3$ (2) in agreement with the value $\approx$5.1, expected on the basis of the amount of active material used in preparation of the sample. This result confirms again that the saturation effects have been properly treated.

Assuming that the Mössbauer f_a factor does not depend on the spin state, the relative percentage $\gamma_{HS-Fe(II)} = \frac{Fe_{HS}^{II}}{Fe_{tot}^{II}}$, which represents the main scope of the present article, was

Table 3. Mossbauer parameters related to the spectra illustrated in figure 7. For all the spectra $\chi^2 \approx 1$ was obtained.

Phase	Component	Mossbauer parameters (mm s^{-1})	$T = 294$ K	$T = 140$ K	$T = 70$ K
HS-Fe(II)	1	δ	0.95(1)	0.97(2)	0.98(5)
		Δ	1.44(4)	1.79(3)	2.0(1)
		σ	0.29(3)	0.10(1)	0.27(6)
		t	0.089(8)	0.3(1)	0.10(2)
	2	δ	0.946(1)	1.1(2)	
		Δ	1.396(1)	1.5(4)	
		σ	0.046(1)	0.154(6)	
		t	0.520(9)	0.8(1)	
LS-Fe(II)	1	δ	0.32(3)	0.4(1)	0.442(1)
		Δ	0.88(5)	0.	0.
		σ	0.001	0.16(4)	0.07(1)
		t	0.008(2)	1.08(1)	2.7(7)
	2	δ			0.442(5)
		Δ			0.3(3)
		σ			0.14(7)
		t			0.6
HS-Fe(II) imp	1	δ	0.99(1)	1.09(1)	1.09(1)
		Δ	2.75(2)	3.15(3)	3.3(1)
		σ	0.06(2)	0.20(2)	0.09(1)
		t	0.027(4)	0.14(1)	0.17(1)

derived from the ratio between the sums of the corresponding thicknesses, apart from the contribution due to the impurity (see above). The thermal dependence of $\gamma_{HS\text{-}Fe(II)}$ is illustrated in figure 10, and it is well represented by the sigmoid function:
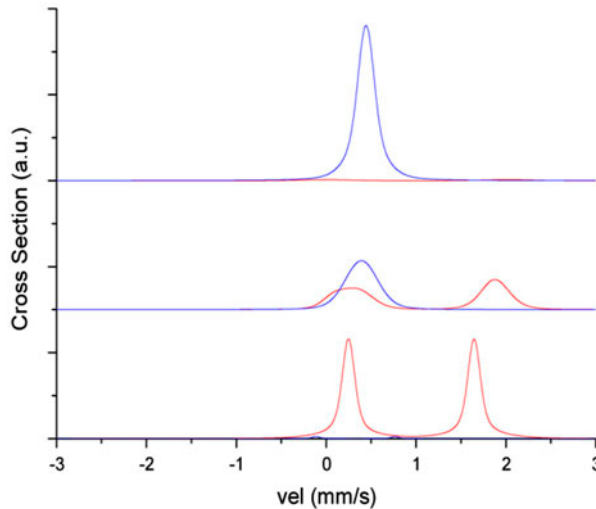

Figure 8. HS and LS contributions to the SCO Mössbauer cross section at 70, 140, and 294 K from top to bottom. Red and blue plots belong to HS-Fe(II) and LS-Fe(II) components, respectively. In the intermediate temperature range, the HS contribution is given by an asymmetrically broadened doublet, as expected on the basis of HS-LS transition times of the order of Γ_n (see http://dx.doi.org/10.1080/00958972.2015.1077951 for color version).
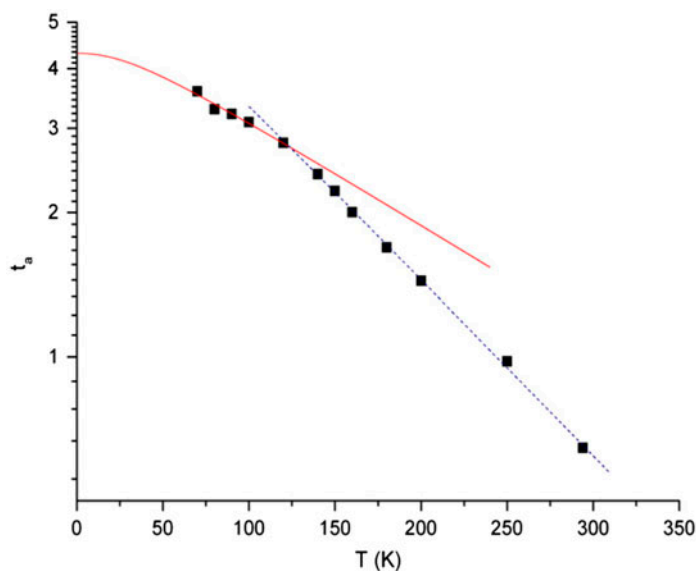
Figure 9. Evolution of the total absorber thickness t_a with T. The experimental points were fitted by means of the Debye model below 120 K (see the text). The dotted line for $T > 120$ K indicates a sharper decrease with respect to the Debye model.

$$\gamma_{HS-Fe(II)} = \left[1 + \exp\left(\frac{\Delta S}{R}\left(\frac{T_{1/2}}{T} - 1\right)\right)\right]^{-1} \tag{2}$$

where $\Delta S/R = 7.0(7)$ and $T_{1/2} = 133(2)$ K, in agreement with magnetic susceptibility measurements, also shown in figure 10. Finally, the quadrupolar splitting values and their increase upon lowering T (see table 3), indicate that the coordination environment of the
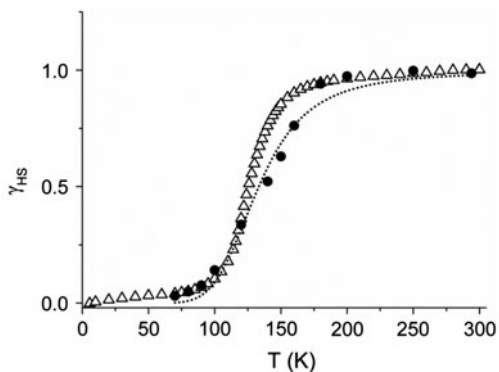

Figure 10. Thermal trend of γHS-Fe(II) for $[Fe(C_6mtz)_6](ClO_4)_2$ derived from Mossbauer (full circles) and SQUID (open triangles) measurements. The dotted line represents the best fit of Mossbauer results by equation (2).

impurity is characterized by an axially compressed octahedral symmetry, as expected according to the Boltzmann population of the Fe(II) ^{5}d orbitals as split by the crystal field [33].

4. Conclusion

A new series of Fe(II) SCO complexes [Fe(C$_6$mtz)$_6$](X)$_2$, where C$_6$mtz is 1-(cyclohexyl-methyl)-1H-tetrazole ligand and X is non-coordinating anion (BF$_4^-$, ClO$_4^-$, or PF$_6^-$), have been synthesized and investigated. The SCO behavior of the small counter-anions BF$_4^-$, ClO$_4^-$ was compared with that of the compound with larger counter-anion PF$_6^-$, and they were found to be considerably different. The PF$_6^-$ compound shows a spin transition at $T_{1/2}$ = 213 K, a considerably higher spin transition temperature (~90 K) than the compounds with the smaller counter-anion BF$_4^-$ ($T_{1/2}$ = 126 K) and ClO$_4^-$ ($T_{1/2}$ = 119 K).

Supplementary material

Supplementary powder diffraction data of **3** and IR spectra of the free ligand and the complexes. CCDC number 1039415 contains the supplementary crystallographic data for this article. These data can be obtained free of charge from The Cambridge Crystallographic Data Center via www.ccdc.cam.ac.uk/data_request/cif.

Acknowledgements

Disclosure statement

No potential conflict of interest was reported by the authors.

Funding

Supplemental data

The supplementary material for this article is available online at http://dx.doi.org/10.1080/00958972.2015.1077951

References

[1] (a) M.A. Halcrow (Ed.). *Spin-Crossover Materials: Properties and Applications*, John Wiley & Sons Ltd, Chichester (2013); (b) O. Khan, J. Kröber, C. Jay. *Adv. Mater.*, **4**, 718 (1992); (c) O. Khan, C.J. Martinez. *Science*, **279**, 44 (1998).

[2] (a) D. Gatteschi, R. Sessoli. *Angew. Chem. Int. Ed.*, **42**, 268 (2003); (b) M. Mannini, F. Pineider, P. Sainctavit, C. Danieli, E. Otero, C. Sciancalepore, A.M. Talarico, M.A. Arrio, A. Cornia, D. Gatteschi, R. Sessoli. *Nat. Mater.*, **8**, 194 (2009); (c) M. Mannini, F. Pineider, C. Danieli, F. Totti, L. Sorace, E.P. Sainctavit, M.A. Arrio, Otero, L. Joly, J.C. Cezar, A. Cornia, R. Sessoli. *Nature*, **468**, 417 (2010); (d) R. Sessoli, M.-E. Boulon, A. Caneschi, M. Mannini, L. Poggini, F. Wilhelm, A. Rogalev. Nat. Phys., **11**, 69 (2015).

[3] J.F. Letard, P. Guionneau, L. Goux-Capes. In *Spin – pCrossover in Transition Metal Compounds III*, P. Gütlich, H.A. Goodwin (Eds), Vol. 235, pp. 221–249, Springer Verlag, Berlin (2004).

[4] V. Niel, A.L. Thompson, A.E. Goeta, C. Enachescu, A. Hauser, A. Galet, M.C. Munoz, J.A. Real. *Chem. Eur. J.*, **11**, 2047 (2005).

[5] M.A. Halcrow. *Polyhedron*, **26**, 3523 (2007).

[6] N. Breufuel, H. Watanabe, L. Toupet, J. Come, N. Matsumoto, E. Collet, K. Tanaka, J.P. Tuchagues. *Angew. Chem. Int. Ed.*, **48**, 9304 (2009).

[7] V. Ksenofontov, A.B. Gaspar, Ph. Gütlich. In *Spin – Crossover in Transition Metal Compounds III*, P. Gütlich, H.A. Goodwin (Eds), Vol. 235, pp. 23–64, Springer Verlag, Berlin (2004).

[8] P. Gütlich, V. Ksenofontov, A.B. Gaspar. *Coord. Chem. Rev.*, **249**, 1811 (2005).

[9] G. Molnár, T. Guillon, N.O. Moussa, L. Rechignat, T. Kitazawa, M. Nardone, A. Bousseksou. *Chem. Phys. Lett.*, **423**, 152 (2006).

[10] J. Jeftić. *High Pressure Res.*, **29**, 369 (2009).

[11] F.L. Yang, B. Li, T. Hanajima, Y. Einaga, R.B. Huang, L.S. Zheng, J. Tao. *Dalton Trans.*, **39**, 2288 (2010).

[12] A. Hauser. In *Spin – Crossover in Transition Metal Compounds II*, P. Gütlich, H.A. Goodwin (Eds), Vol. 234, pp. 155–198, Springer Verlag, Berlin (2004).

[13] V. Legrand, S. Pillet, C. Carbonera, M. Souhassou, J.-F. Letard, P. Guionneau, C. Lecomte. *Eur. J. Inorg. Chem.*, **36**, 5693, (2007).

[14] C. de Graaf, C. Sousa, *Chem. Eur. J.*, **16**, 4550 (2010).

[15] A. Bousseksou, F. Varret, M. Goiran, K. Boukheddaden, J.P. Tuchagues. In*Spin – Crossover in Transition Metal Compounds III*, P. Gütlich, H.A. Goodwin (Eds), Vol. 235, pp. 65–84, Springer Verlag, Berlin (2004).

[16] L. Cambi, L. Szegö. *Ber. Dtsch. Chem. Ges.*, **64**, 2591 (1931).

[17] P. Gütlich, H.A. Goodwin (Eds). *Spin – Crossover in Transition Metal Compounds I-III*, Springer Verlag, Berlin (2004).

[18] (a) A. Tissot, P. Fertey, R. Guillot, V. Briois, M.-L. Boillot. *Eur. J. Inorg. Chem.*, **101** (2014); (b) C. Kruger, P. Augustin, L. Dlhan, J. Pavlik, J. Moncol, I. Nemec, R. Boca, F. Renz. *Polyhedron*, **87**, 194 (2015).

[19] M.G. Cowan, J. Olguín, S. Narayanaswamy, J.L. Tallon, S. Brooker. *J. Am. Chem. Soc.*, **134**, 2892 (2012).

[20] Y. Garcia, P. Gütlich. In *Spin – Crossover in Transition Metal Compounds II*, P. Gütlich, H.A. Goodwin (Eds), Vol. 234, pp. 49–62, Springer Verlag, Berlin (2004).

[21] (a) M. Tafili-Kryeziu, M. Weil, T. Muranaka, A. Bousseksou, M. Hasegawa, A. Jun, W. Linert. *Dalton Trans.*, **42**, 15796 (2013); (b) M. Quesada, F. Prins, E. Bill, H. Koojiman, P. Gamez, O. Roubeau, A.L. Spek, J.G. Haasnoot, J. Reedijk. *Chem. Eur. J.*, **14**, 8486 (2008).

[22] A. Soliman, M. Khattab, M. Reissner, P. Weinberger, F. Werner, W. Linert. *Inorg. Chim. Acta*, **360**, 3987 (2007).

[23] N. Hassan, P. Weinberger, F. Kubel, G. Molnar, A. Bousseksou, L. Dlhan, R. Boča, W. Linert. *Inorg. Chim. Acta*, **362**, 3629 (2009).

[24] G. Spina, M. Lantieri. *Nucl. Instrum. Methods*, **318**, 253 (2014).

[25] G.J. Long, T.E. Cranshaw, G. Longworth. *Mössbauer Effect Ref. Data J.*, **6**, 42 (1983).

[26] C. Janot. *The Mossbauer Effect and its Applications*, Masson et C.ie, Paris (1972).

[27] J. Blomquist. *Nucl. Instr. Meth. Phys. Res.*, **218**, 253 (2014).

[28] Bruker. *APEX2, SAINT and SADABS*, Bruker AXS Inc., Madison (2010).

[29] G.M. Sheldrick. *Acta Crystallogr. A*, **64**, 112 (2008).

[30] T. Kamiya, Y. Saito. *Ger. Pat*, 2147023 (1973).

[31] D.Rancourt. In *Mössbauer Spectroscopy Applied to Magnetism and Materials Science*, G. Long, F. Grandjean (Eds), Vol. 2, Plenum Press, New York, NY (1996).

[32] G. Spina, L. Cianchi. In *NMR-MRI, mSR and Mössbauer Spectroscopies in Molecular Magnets*, P. Carretta, A. Lascialfari (Eds), pp. 249–275, Springer-Verlag, Milano (2007).

[33] G.M. Bancroft. *Mössbauer Spectroscopy: An Introduction for Inorganic Chemists and Geochemists*, McGraw-Hill, London (1973).